PHYSICS

Correction for "Distortions and stabilization of simple-cubic calcium at high pressure and low temperature," by Wendy L. Mao, Lin Wang, Yang Ding, Wenge Yang, Wenjun Liu, Duck Young Kim, Wei Luo, Rajeev Ahuja, Yue Meng, Stas Sinogeikin, Jinfu Shu, and Ho-kwang Mao, which appeared in issue 22, June 1, 2010, of *Proc Natl Acad Sci USA* (107:9965–9968; first published May 17, 2010; 10.1073/pnas.1005279107).

The authors note that due to a printer's error, the affiliation information for Wendy L. Mao was incorrect. The correct institution name is SLAC.

The authors would also like to note that Fig. 5 was incorrect as shown. The corrected figure and its legend appear below.

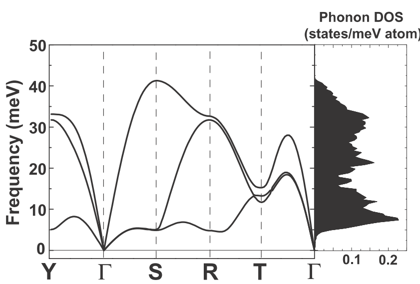

Fig. 5. Phonon dispersion relation (*Left*) and density of states (DOS) (*Right*) for pm Ca-VI.

MICROBIOLOGY

Correction for "Chemical sensing in mammalian host-bacterial commensal associations," by David T. Hughes, Darya A. Terekhova, Linda Liou, Carolyn J. Hovde, Jason W. Sahl, Arati V. Patankar, Juan E. Gonzalez, Thomas S. Edrington, David A. Rasko, and Vanessa Sperandio, which appeared in issue 21, May 25, 2010, of *Proc Natl Acad Sci USA* (107:9831–9836; first published May 10, 2010; 10.1073/pnas.1002551107).

The authors note that the following statement should be added to the Acknowledgments: "V.S. was supported by National Institutes of Health Grant AI077613."

NEUROSCIENCE

Correction for "GluN2B subunit-containing NMDA receptor antagonists prevent Aβ-mediated synaptic plasticity disruption in vivo," by Neng-Wei Hu, Igor Klyubin, Roger Anwy, and Michael J. Rowan, which appeared in issue 48, December 1, 2009, of *Proc Natl Acad Sci USA* (106:20504–20509; first published November 16, 2009; 10.1073/pnas.0908083106).

The authors note that the author name Roger Anwy should have appeared as Roger Anwyl. The corrected author line appears below. The online version has been corrected.

Neng-Wei Hu[a,b], Igor Klyubin[a,b], Roger Anwyl[b,c], and Michael J. [a,b,1]

Distortions and stabilization of simple-cubic calcium at high pressure and low temperature

Wendy L. Mao[a,b,c,1], Lin Wang[d], Yang Ding[d], Wenge Yang[d,e], Wenjun Liu[f], Duck Young Kim[g,h], Wei Luo[g,i], Rajeev Ahuja[g,i], Yue Meng[e], Stas Sinogeikin[e], Jinfu Shu[j], and Ho-kwang Mao[d,e,j,1]

[a]Geological and Environmental Sciences, Stanford University, Stanford, CA 94305; [b]Photon Science and [c]Stanford Institute for Materials and Energy Sciences, Stanford Linear Accelerator Center National Accelerator Laboratory, Menlo Park, CA 94025; [d]High Pressure Synergetic Consortium and [e]High Pressure Collaborative Access Team, Carnegie Institution of Washington, Argonne, IL 60439; [f]X-ray Operations and Research, Advanced Photon Source, Argonne National Laboratory, Argonne, IL 60439; [g]Condensed Matter Theory Group, Department of Physics, Uppsala University, Uppsala, Sweden; [h]Theory of Condensed Matter Group, Cavendish Laboratory, Cambridge CB3 0HE, United Kingdom; [i]Department of Materials Science and Engineering, Royal Institute of Technology, Stockholm, Sweden; and [j]Geophysical Laboratory, Carnegie Institution of Washington, Washington, DC 20015

Contributed by Ho-Kwang Mao, April 19, 2010 (sent for review March 10, 2010)

Ca-III, the first superconducting calcium phase under pressure, was identified as simple-cubic (sc) by previous X-ray diffraction (XRD) experiments. In contrast, all previous theoretical calculations showed that sc had a higher enthalpy than many proposed structures and had an imaginary (unstable) phonon branch. By using our newly developed submicrometer high-pressure single-crystal XRD, cryogenic high-pressure XRD, and theoretical calculations, we demonstrate that Ca-III is neither exactly sc nor any of the lower-enthalpy phases, but sustains the sc-like, primitive unit by a rhombohedral distortion at 300 K and a monoclinic distortion below 30 K. This surprising discovery reveals a scenario that the high-pressure structure of calcium does not go to the zero-temperature global enthalpy minimum but is dictated by high-temperature anharmonicity and low-temperature metastability fine-tuned with phonon stability at the local minimum.

high pressure | phase transition | superconductivity

Advances in high-pressure research as a result of the interplay between theory and experiments have revealed unique physics in simple elements (1–5). The series of surprising high-pressure phase transitions (6–9) that change the elemental Ca from an ordinary metal to the highest known T_c (>25 K) elemental superconductor (8) has emerged as a central topic as demonstrated in many concurrent investigations (10–17) but also presented a seemingly irreconcilable gap between theory and experiment. X-ray diffraction (XRD) at 300 K indicates that Ca transforms from its ambient condition fcc structure Ca-I to body-centered cubic (bcc) Ca-II at 20 GPa and then to simple-cubic (sc) Ca-III at 32 GPa (7, 9, 18). At higher pressures, Ca-III undergoes two additional transformations, to Ca-IV and V at 119 and 143 GPa, respectively (7, 9, 18). Ca-III, IV, and V are all superconducting (8).

Ca-III is perhaps the most enigmatic and intriguing phase in this series. It is the first superconducting phase of Ca (6, 8) and exhibits a large T_c increase with pressure from 2 to 10 K (8). The transition sequence from Ca-I to II to III is counterintuitive from a close-packed sphere concept, because it represents a decrease in coordination from 12 to 8 to 6 with increasing density (12). Although sc has a lower enthalpy than the bcc and fcc phases (19), theoretical calculations have found a number of structures that have lower zero-temperature enthalpy than sc and have shown that the sc should not have existed because of phonon instability (11, 12, 14, 17). Yet sc was the only phase observed in all previous high-pressure XRD experiments between 33 and 110 GPa (7, 9, 16).

In calculations, Teweldeberhan and Bonev (14) discovered two lower-enthalpy (than sc) orthorhombic Ca phases, *Cmcm* and *Pnma*, for temperatures up to the melting point (20), and Yao et al. (17) discovered a tetragonal $I4_1/amd$ structure that is the lowest-enthalpy phase at zero temperature. These proposed structures have not been observed experimentally. Very recently, Gu et al. conducted an accurate powder XRD study and confirmed again the good agreement of Ca-III with the sc indexing (16). Some differences between experiment and theory may be explained by anharmonicity at room temperature and the absence of low-temperature, high-pressure XRD experiments. Some of the most perplexing questions, however, remain unanswered.

Whereas the primitive sc unit cell is the simplest possible atomic arrangement for elements, it is rare and generally considered unfavorable from the standpoint of a hard-sphere model (imagine stacking a ball directly on top of another ball), particularly under stress. Why then is sc observed in all experiments? Is the sc phase superconducting? What happens to the "collapsed" structure when it has imaginary phonon branches? Most fundamentally, if the phonon-unstable, high-enthalpy, sc Ca could persist to near-zero temperature where the anharmonic argument could no longer help, we would have to reconsider the assumptions and theories used in searching for the lowest-enthalpy phase and calculating the phonon band structure.

Results and Discussion

To unravel this enigma, we conducted a series of experimental and theoretical investigations on Ca-III and determined the structure up to 50 GPa at temperatures from 300 to 4 K, by using synchrotron powder XRD and a submicrometer single-crystal XRD technique. Powder XRD patterns were collected at 300 K upon increasing pressure. We observed the transitions from fcc (Ca-I) to bcc (Ca-II) at 20 GPa and then from Ca-II to Ca-III above 33 GPa, consistent with previous observations. Previous assignments of the sc structure were based on five XRD peaks (7, 9, 16). To improve the confidence level, we greatly expanded the accessibility range by using the 70°-opening plate diamond-anvil cell (DAC) (21) and collected thirteen XRD peaks of Ca-III. All thirteen observed d spacings down to 0.7 Å show excellent agreement with sc unit cell ($a = 2.6750(5)$ Å) (see Table S1), apparently a reconfirmation of sc.

However, a closer examination reveals an anomaly in the XRD pattern (Fig. 1). Whereas the $h00$ peaks are very narrow, other reflections show broadening. This feature is reminiscent of the rhombohedral (rh) distortion of the cubic lattice [e.g., vanadium (22)]. The Miller indices hkl are identical for sc and rh, and the only change is $\alpha = \beta = \gamma \neq 90°$ in rh. In sc, the d spacings are degenerate and indistinguishable in powder XRD for all

Author contributions: W.L.M. and H.-K.M. designed research; W.L.M., L.W., Y.D., W.Y., W. Liu, D.Y.K., W. Luo, R.A., Y.M., S.S., and J.S. performed research; W.Y. and W. Liu contributed new reagents/analytic tools; W.L.M., D.Y.K., W. Luo, and R.A. analyzed data; and W.L.M., D.Y.K., R.A., and H.-K.M. wrote the paper.

The authors declare no conflict of interest.

[1]To whom correspondence may be addressed. E-mail: wmao@stanford.edu or mao@gl.ciw.edu.

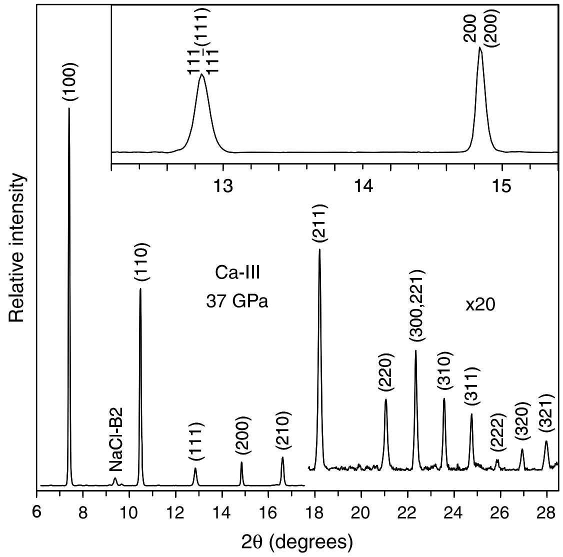

Fig. 1. Integrated powder XRD pattern for rh Ca-III at 37 GPa and 300 K ($\lambda = 0.39585$ Å) collected at beamline 16-IDB of the Advanced Photon Source (APS), Argonne National Laboratory. For clarity sc indexing is shown (the corresponding rh indexing is given in Table S1). The small d spacing (large 2θ) region is magnified 20×. The inset shows clear broadening in what would be the sc body diagonal 111 but is in fact a doublet corresponding to the rh 111 and $1\bar{1}1$, compared to the h00 reflections, which remain very sharp.

permutations and sign changes of h, k, and l; in rh, sign differences, except the Friedel mates, change the d spacings and result in peak broadening or splitting as the rh α angle deviates from 90°. In Fig. 1, the 111 is clearly broadened compared to the 200, as would be expected for a distorted rh in which the d spacings for 111 and $1\bar{1}1$ diverge into an unresolved broad peak while the rh 200 remains degenerate as a single sharp peak. Whereas such peak width comparison reveals the possibility of rh distortion, it lacks the resolution needed for small degrees of distortion. It would be valuable to conduct single-crystal XRD in which different hkl permutations and signs would appear as separate spots in reciprocal space, rather than an unresolved broad peak as in powder XRD; very slight differences in d spacing could be readily and quantitatively resolved.

In an attempt to grow a single crystal of Ca-III and to relieve deviatoric stress below the detection limit (0.3 GPa), a double-sided Nd:YLF laser-heating system was used to anneal the sample to 1,000 K for 30 min. By using the 7×7 μm X-ray beam at 16ID-B, the XRD pattern after heating is spotty (Fig. 1), but the estimated maximum crystallite size of 1 μm is still far from useful for existing high-pressure single-crystal XRD techniques. To overcome this problem, we developed a single-crystal XRD technique by using a 600-nm focused beam to pick a single crystallite in the polycrystalline aggregate and collect single-crystal XRD data. Fig. 2 shows the XRD zone pattern of a Ca single crystallite at 42 GPa. The geometric relations of the reciprocal lattice indicate that the crystallite has a nearly sc unit cell. Following its orientation matrix, different diffraction spots of the (pseudo)sc crystallite are resolved; e.g., 300 and 221 reflections that overlap in powder pattern appear as different spots in single-crystal diffraction. The h00 reflections always appear as sharp single spots with a single d spacing, whereas other reflections appear as multiple twin spots with different d spacings that define the rh distortion (see Table S2 for a summary of single-crystal data). The rh cell retains the cubic relation $a = b = c = 2.6684(5)$ Å but relaxes the 90° angular constraint to $\alpha = \beta = \gamma = 89.90(1)°$. The powder XRD pattern observed with the 7×7 μm beam is compared with the rh indexing (see Fig. 1 and Table S1) and shows excellent agreement in both peak positions and peak

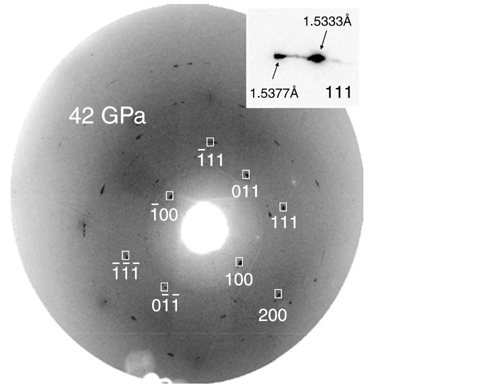

Fig. 2. Single-crystal zone pattern for Ca-III at 42 GPa and 300 K by using submicrometer beam at 34-ID, APS. Single-crystal spots are indexed to a rh structure. The inset shows splitting of the cubic 111 peak.

widths. In conclusion, at 300 K above 32 GPa, Ca transforms from bcc to rh phase with a sc-like primitive unit cell exhibiting a rh distortion.

The small rh distortion is insufficient to overcome the phonon-instability constraint at 0 K. To investigate the Ca-III low-temperature stability, the same sample in the plate DAC was cooled in a liquid helium cryostat. Powder XRD patterns were collected during cooling down to 4.3 K through double windows of single-crystal sapphire cryostat windows that contribute to some intense single-crystal background spots on the XRD image (Fig. 3). The XRD patterns remain sc-like throughout the entire pressure-temperature range. We did not observe any of the theoretically proposed lower-enthalpy, larger-unit cell phases, including *Cmcm*, *Pnma* (14), *Pnma*, and $I4_1/amd$ (17).

Below 30 K, the rh phase transforms to another sc-like phase that is still based on the primitive sc unit cell but with a different, larger distortion in which one of the *a-b* face diagonals of the primitive sc cell expands by 2%, and the other diagonal shrinks

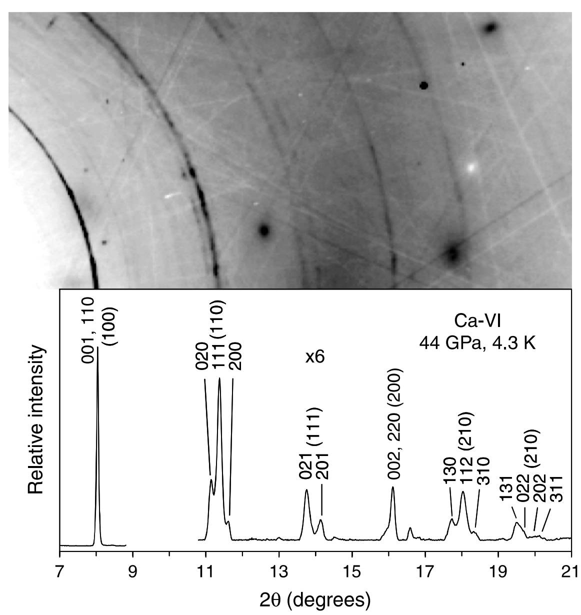

Fig. 3. Integrated polycrystalline XRD pattern at 44 GPa and 4.3 K ($\lambda = 0.36940$ Å) collected at 16-IDB, APS. Peaks are indexed both to the orthorhombic structure and also to sc (in parentheses) for reference. The small d spacing (large 2θ) region is magnified 6×. There were no reflections with 2θ less than 8°. The two-dimensional XRD image is shown at top. Single-crystal spots from the sapphire cryostat windows and diamond anvils have been masked out.

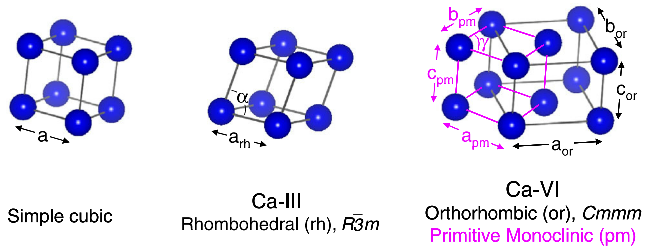

Fig. 4. Models of the proposed crystal structures for rh Ca-III and orthorhombic Ca-VI (pm unit cell is shown in pink). The rh distortion is exaggerated so that the fact that the angle $\alpha \neq 90°$ is obvious.

by 2% while c remains perpendicular to the a-b plane, forming a primitive monoclinic (pm) unit cell with $a = b = 2.6373(7)$ Å, $c = 2.6350(8)$ Å, $\alpha = \beta = 90°$, and $\gamma = 87.62(1)°$. Again, the Miller indices are identical in sc and pm because the same primitive cell is chosen, but the different permutations and sign changes of *hkl* result in peak splitting. As show in Fig. 3 and Table S3, the observed XRD pattern is in excellent agreement with the pm indexing (all $\Delta d/d < 0.001$). The special case of $a = b$ in this pm allows the choice of a higher-symmetry, larger, orthorhombic, c-face-centered unit cell of *Cmmm* space group with $a = 3.6513(10)$ Å, $b = 3.8064(10)$ Å, and $c = 2.6350(8)$ Å (see Fig. 3 and Table S3 for comparison calculated and observed d spacings). Superconducting Ca above 32 GPa is therefore pm or *Cmmm*, not sc or rh. The relationship between sc and its rh and pm distorted primitive cells are illustrated in Fig. 4. In a separate reconnaissance study, we found that when bcc Ca-II is compressed at low temperature, it converts directly into pm.

The dynamical stability of the pm Ca phase was analyzed on the basis of ab initio lattice dynamics as implemented in ABINIT software (23). Fig. 5 shows the stabilized phonon dispersion relations and the corresponding phonon density of states. Phonon dispersion curves were calculated along the $Y(\frac{1}{2}\,\frac{1}{2}\,0) - \Gamma(0\,0\,0) - S(\frac{1}{2}\,0\,0) - R(\frac{1}{2}\,0\,\frac{1}{2}) - T(\frac{1}{2}\,\frac{1}{2}\,\frac{1}{2}) - \Gamma(0\,0\,0)$ high symmetry points. Energetically, by starting from sc, both rh or pm distortions tend to lower the enthalpy around this pressure. For example, at 40 GPa, pm is calculated to lower enthalpy of sc by 19 meV. Therefore, our experimental observations of the pm distortion of the sc phase are consistent with the calculation. On the other hand, the ground state $I4_1/amd$ is calculated to be 42 meV lower than pm; this remains enigmatic.

In conclusion, whereas many structures, typically with larger unit cells of 4–8 atoms per cell, have been proposed (12–15, 17) to have lower zero-temperature enthalpies than sc, Ca remains in its simplest form with one atom per primitive unit cell. Given the rh to pm transition at low T, it is clear that at 300 K, anharmonic and entropic contributions play a significant role for the stabilization of the sc-like rh phase. Below 30 K, the kinetics are insufficient to overcome the energy barrier that prevents the transition of the sc-like primitive cell into other lowest-enthalpy phases. In response to the phonon instability, the primitive cell simply distorts slightly into a nearby phonon-stable form. This flexibility creates the interesting scenario of Ca that the standard approach of searching for global enthalpy minimum at zero temperature no longer defines the structure that is trapped within the vicinity of the sc local enthalpy minimum. The pressure-induced Fermi surface nesting that causes phonon instability (11, 24, 25) and a variety of lattice distortions that marginally restore phonon stability also generates the rich phonon anomaly behavior (26) and produces the two highest elemental T_cs [i.e., V at 17.2 K (27) and Ca at 25 K (8)].

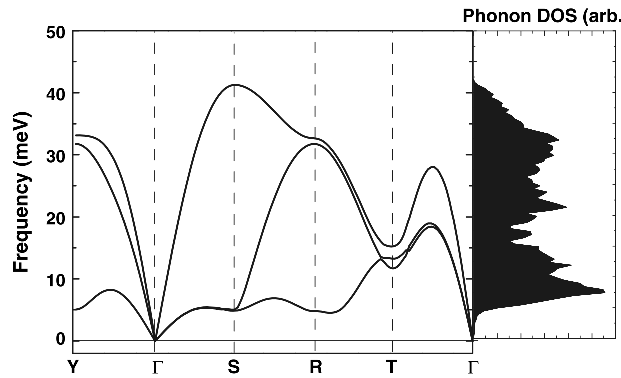

Fig. 5. Phonon dispersion relation (*Left*) and density of states (DOS) (*Right*) for pm Ca-VI.

Materials and Methods

A plate DAC (21) with 300 μm flat-culet diamonds was used for pressurization and X-ray probing access through the 70° axial opening. The sample assemblage was composed of Ca (99.98% purity from Alfa Aesar) sandwiched between thin (7-μm) layers of NaCl, which acted as a thermal insulator and pressure-transmitting medium, along with a small ruby chip whose fluorescence was measured for determining pressure. The sample was loaded, into a ~100 μm diameter chamber that was drilled into a preindented Re gasket in a glove box to avoid oxidation.

The phonon calculations are based on the generalized gradient approximation with the Perdew–Burke–Ernzerhof parameterization (28) for the exchange-correlation functional to density functional perturbation theory (29) with a kinetic energy cutoff 50 Hartrees. To calculate phonon dispersion relations, a $12 \times 12 \times 12$ Monkhorst–Pack (30) mesh was found to yield converged results with Hartwigsen–Goedecker–Hutter pseudopotentials (31). Phonon calculations were performed on an $8 \times 8 \times 8$ Monkhorst–Pack mesh with a $16 \times 16 \times 16$ mesh for the first Brillouin zone integration.

ACKNOWLEDGMENTS. This work is supported by the Department of Energy, Office of Basic Energy Sciences (DOE-BES), Division of Materials Sciences and Engineering, under Contract DE-AC02-76SF00515. HPSynC is supported as part of the EFree, an Energy Frontier Research Center funded by DOE-BES under Award DE-SC0001057. HPCAT is supported by DOE-BES, DOE-National Nuclear Security Administration (Carnegie/Department of Energy Alliance Center), and National Science Foundation. Use of the APS was supported by DOE-BES under Contract DE-AC02-06CH11357. D.Y.K. and R.A. acknowledge Wenner-Gren stiftelserna for financial support and Swedish National Infrastructure for Computing and Uppsala Multidisciplinary Center for Advanced Computational Science for providing computer time.

1. Gregoryanz E, et al. (2008) Structural diversity of sodium. *Science* 320:1054–1057.
2. Matsuoka T, Shimizu K (2009) Direct observation of a pressure-induced metal-to-semiconductor transition in lithium. *Nature* 458:186–189.
3. Ashcroft NW (2009) Condensed-matter physics: Pressure for change in metals. *Nature* 458(12 Mar):158–159.
4. Ma Y, et al. (2009) Transparent dense sodium. *Nature* 458:182–185.
5. Oganov AR, et al. (2009) Ionic high-pressure form of elemental boron. *Nature* 457:863–867.
6. Dunn KJ, Bundy FP (1981) Electrical-resistance behavior of Ca at high pressures and low temperatures. *Phys Rev B* 24(4):1643–1650.
7. Olijnyk H, Holzapfel WB (1984) Phase transitions in alkaline earth metals under pressure. *Phys Lett A* 100(4):191–194.
8. Yabuuchi T, Matsuoka T, Nakamoto Y, Shimizu K (2006) Superconductivity of Ca exceeding 25 K at megabar pressures. *J Phys Soc Jpn* 75(8):083701–083703.
9. Yabuuchi T, Nakamoto Y, Shimizu K, Kikegawa T (2005) New high-pressure phase of calcium. *J Phys Soc Jpn* 74(9):2391–2392.
10. Arapan S, Mao HK, Ahuja R (2008) Prediction of incommensurate crystal structure in Ca at high pressure. *Proc Natl Acad Sci USA* 105(52):20627–20630.
11. Errea I, Martinez-Canales M, Oganov AR, Bergara A (2008) Fermi surface nesting and phonon instabilities in simple cubic calcium. *High Press Res* 28(4):443–448.
12. Gao G, et al. (2008) Electronic structures, lattice dynamics, and electron-phonon coupling of simple cubic Ca under pressure,. *Solid State Commun* 146:181–185.
13. Ishikawa T, et al. (2008) Theoretical study of the structure of calcium in phases IV and V via ab initio metadynamics simulation. *Phys Rev B* 77:020101.
14. Teweldeberhan AM, Bonev SA (2008) High-pressure phases of calcium and their finite-temperature phase boundaries. *Phys Rev B* 78:140101.
15. Yao Y, et al. (2008) Structures and superconducting properties of the high-pressure IV and V phases of calcium from first principles. *Phys Rev B* 78:054506.

16. Gu QF, Krauss G, Grin Y, Steurer W (2009) Experimental confirmation of the stability and chemical bonding analysis of the high-pressure phases Ca-I, II, and III at pressures up to 52 GPa. *Phys Rev B* 79:134121.
17. Yao Y, Klug DD, Sun J, Martonňák R (2009) Structural prediction and phase transformation mechanisms in calcium at high pressure. *Phys Rev Lett* 103:055503.
18. Fujihisa H, Nakamoto Y, Shimizu K, Yabuuchi T, Gotoh Y (2008) Crystal structures of calcium IV and V under high pressure. *Phys Rev Lett* 101:095503.
19. Ahuja R, Eriksson O, Wills JM, Johansson B (1995) Theoretical confirmation of the high pressure simple cubic phase in calcium. *Phys Rev Lett* 75(19):3473–3476.
20. Errandonea D, Boehler R, Ross M (2001) Melting of the alkaline-earth metals to 80 GPa. *Phys Rev B* 65(13):012108.
21. Boehler R (2006) New diamond cell for single-crystal x-ray diffraction. *Rev Sci Instrum* 77(11):115103.
22. Ding Y, et al. (2007) Structural phase transition of vanadium at 69 GPa. *Phys Rev Lett* 98:085502.
23. Gonze X, et al. (2002) First-principles computation of material properties: The ABINIT software project. *Comp Mater Sci* 25:478–492.
24. Landa A, et al. (2006) Fermi surface nesting and pre-martensitic softening in V and Nb at high pressures. *J Phys: Condens Matter* 18:5079–5085.
25. Luo W, Ahuja R, Ding Y, Mao HK (2007) Unusual lattice dynamics of vanadium under high pressure. *Proc Natl Acad Sci USA* 104(42):16428–16431.
26. Suzuki N, Otani M (2007) The role of the phonon anomaly in the superconductivity of vanadium and selenium under high pressures. *J Phys: Condens Matter* 19:125206.
27. Ishizuka M, Iketani M, Endo S (2000) Pressure effect on superconductivity of vanadium at megabar pressures. *Phys Rev B* 61(6):R3823–R3825.
28. Perdew JP, Burke K, Ernzerhof M (1996) Generalized gradient approximation made simple. *Phys Rev Lett* 77(18):3865–3868.
29. Baroni S, de Gironcoli S, Dal Corso A (2001) Phonons and related crystal properties from density-functional perturbation theory. *Rev Mod Phys* 73(2):515–562.
30. Monkhorst HJ, Pack JD (1976) Special points for Brillouin-zone integrations. *Phys Rev B* 13(12):5188–5192.
31. Krack M (2005) Pseudopotentials for H to Kr optimized for gradient-corrected exchange-correlation functionals. *Theor Chem Acc* 114:145–152.